Eur. Phys. J. B **10**, 361–370 (1999)

THE EUROPEAN PHYSICAL JOURNAL B

EDP Sciences

Quantum corrections to the conductance of a square quantum dot with soft confinement

T. Ouchterlony[1], I.V. Zozoulenko[1,a], C.-K. Wang[1], K.-F. Berggren[1], C. Gould[2], and A.S. Sachrajda[2]

[1] Department of Physics and Measurement Technology, Linköping University, 581 83 Linköping, Sweden
[2] National Research Council Canada, Institute for Microstructural Science, Ottawa K1A 0R6, Canada

Received 13 May 1998

Abstract. We study the conductance of a square quantum dot, modeling the potential with a self-consistent Thomas-Fermi approximation. The resulting potential is characterized by level statistics indicative of mixed chaotic and regular electron dynamics within the dot in spite of the regular geometry of the gates defining the dot. We calculate numerically, for the case of a quantum dot with soft confinement, the weak localization (WL) correction. We demonstrate that this confining potential may generate either Lorentzian or linear lineshapes depending on the number of modes in the leads. Finally, we present experimental WL data for a lithographically square dot and compare the results with numerical calculations. We analyze the experimental results and numerical simulations in terms of semiclassical and random matrix theory (RMT) predictions and discuss their limitations as far as real experimental structures are concerned. Our results indicate that direct application of the above predictions to distinguish between chaotic and regular dynamics in a particular cavity can not always lead to reliable conclusions as the shape and magnitude of the WL correction can be strongly sensitive to the geometry-specific, non-universal features of the system.

PACS. 73.23.-b Mesoscopic systems – 73.20.Fz Weak or Anderson localization – 73.23.Ad Ballistic transport

1 Introduction

Various aspects of the electrical conductance through quantum dots and other mesoscopic structures have been studied extensively both experimentally and theoretically since the technology of fabricating such structures was developed (for a review, see [1]). An interesting example is the ballistic motion of electrons through a quantum dot, which occurs when the geometrical size of the dot is smaller than the elastic and inelastic mean free paths of the electrons. In this case the geometrical shape of the potential, rather than disorder-induced scattering and/or electron-electron interactions determine the transport properties of the phase-coherent electrons in the dot. Recently a number of semiclassical predictions have been made regarding the statistical properties of quantum conduction fluctuations. In particular, Baranger *et al.* [2] have shown that the ballistic weak localization (WL) effect, is sensitive to the shape of the system. The terminology of weak localization is introduced for this kind of systems in direct analogy with the coherent backscattering effects typical for disordered systems and the associated self-averaging over different impurity configurations. In the present case, however, the role of impurities is replaced by the geometry of the device and an averaging over samples/devices or energy is performed instead of impurity configurations. Specifically, for quantum dots whose classical counterparts generate chaotic dynamics, the semiclassical approach of Baranger *et al.* [2] gives a Lorentzian shape of the energy-averaged WL peak,

$$\langle R(B)\rangle = R_0 + \Delta R/[1 + (2B/\alpha\phi_0)^2] \qquad (1)$$

whereas for non-chaotic (regular) cavities the lineshape is linear

$$R_0 - \langle R(B)\rangle \propto |B|. \qquad (2)$$

R_0 is the average reflection coefficient without weak localization effects, ΔR the correction for $B = 0$, $\phi_0 = h/e$ the flux quantum, and $\alpha = (2\pi S)^{-1}$ the inverse of the typical area S times 2π. The magnitude of the weak localization correction ΔR has been estimated within a random $S-$matrix theory (RMT) [3–9] and the semiclassical approach [10] and is shown to depend on the number of modes in the leads, the strength of the coupling, the symmetry of the structure and the phase-breaking time.

These theoretical studies stimulated a large amount of experimental activity. Up to date, a number of groups have reported WL measurements in quantum dots with a wide variety of shapes [11–18]. Some of these studies have even been included in recent textbooks and a review as examples of a transition from integrability to chaos

[a] e-mail: igorz@ifm.liu.se

[3,19,20]. However, it remains the case that the interpretation of the above experiments is controversial.

Indeed, the first systematic experimental study of the WL shape in the chaotic (stadium-shaped) and regular (circular) quantum dots was reported by Chang *et al.* [11]. In agreement with the semiclassical predictions they found a Lorentzian WL shape for the chaotic situation and a linear shape for the case of a regular dot. However, this experiment still remains the only one where the expected difference was positively identified. In the subsequent experiments of Berry *et al.* [12] and Lee *et al.* [18] on a similar circular dot with the same lead positions, a Lorentzian WL peak shape was observed (instead of the expected linear one). Moreover, Lütjering *et al.* [16] and Lee *et al.* [18] reported linear WL peaks for a variety of chaotic structures [21] (instead of the expected Lorentzian ones). In the recent experiment by Keller *et al.* [17] a Lorentzian-shaped WL peak was found for both chaotic and regular cavities. However, it is worth stressing that while the WL shape is not always consistent with semiclassical predictions, the effective area of the dot, as extracted from the fitting to the Lorentzian (1), is often in a good agreement with the actual area of the dot deduced from the lithographical shape, high-field Aharonov-Bohm oscillations etc.

This brief review of existing experimental results demonstrates that further studies are clearly required to answer one of the central questions in this field. Namely, is it possible, on the basis of the experimentally observed WL lineshape (Lorentzian *vs.* linear), to make a definite conclusion about the character of the underlying classical electron dynamics (*i.e.* chaotic *vs.* regular)?

In this paper we attempt to answer this question for a case that mimics experimental realities. The first important aspect is that we take only a small number of opens channels into account. As opposed to the usual numerical approach where a hard-wall confining potential is assumed, we start with the lithographical shape of the gates and calculate self-consistently the realistic potential inside the dot using the Thomas-Fermi approximation. We perform a detailed numerical analysis of the effect of the soft confining potential on the character of the conductance oscillations. To the best of our knowledge this aspect of electron transport in quantum dots has not been addressed to date in the literature. We note that recent papers have stressed the important consequences of soft-wall potentials in nanostructures with regard to changes in the level statistics [22] and the fractal nature of conductance fluctuations [23].

Transport characteristics of an open structure (chaotic *vs.* regular) are usually analyzed on the basis of the corresponding properties of the related closed structure. In addition, the nominal shape of the lithographic gates is usually used to draw conclusions on the character of electron dynamics within the dot. We show that this approach may be misleading as far as the electron dynamics of the actual dot is concerned. In particular, we calculate the level spacing statistics for the realistic confining potential inside a nominally (*i.e.* lithographically) square dot. Considerable level repulsion in the energy spectrum indicates the presence of irregular behavior. The corresponding level statistics is found to be effectively in between the Poisson and Wigner distributions, *i.e.*, the dynamics is mixed – both regular and chaotic aspects are present. This is in contrast to the regular dynamics of the ideal square billiard.

Finally, we investigate, both theoretically and experimentally, the ballistic weak localization correction of a nominally square dot. In contrast to many experiments where a comparison with the semiclassical theory has been performed using energy or ensemble averaging, we use temperature averaging in a single dot. As shown in previous work [24], if the temperature is raised so that Ohmic addition is established in the dot and the conductance oscillations are smeared out, temperature averaging is equivalent to energy averaging (in the sense that a comparison with semiclassical predictions becomes meaningful). The results of reference [24] were used to analyze experimental data of Bird *et al.* [15] which were obtained for a *single* square dot in the extreme quantum regime of very low temperature (up to $\sim$ 25 mK). It was shown that in this regime an interpretation of the observed shapes of the WL curves on the basis of the semiclassical predictions becomes ambiguous, because the condition for the validity of the latter has not been met. Numerical simulations of reference [24] demonstrate that, in agreement with the semiclassical theory, the WL corrections for an ideal square dot have typically a linear lineshape. It was also shown that deviations from perfect square confinement may have a significant effect on the detailed shape of the WL curve. In the present work we go beyond the hard-wall confinement model used in [24] and perform numerical calculations for the WL peak for the realistic self-consistent potential. We demonstrate that this confining potential may generate either a Lorentzian or a linear lineshape depending on the number of modes in the leads. Finally, we present our experimental data of the temperature-averaged ballistic weak localization of a square quantum dot and compare it to the results of numerical calculations. We analyze the experimental results and numerical simulations in terms of semiclassical and the RMT approaches and discuss their limitations in detail as far as realistic experimental structures are concerned.

2 Modeling of the quantum dot and the self-consistent confining potential

In modeling the dot we assume that it is fabricated from a modulation-doped $Al_xGa_{1-x}As/GaAs$ heterostructure with a planar interface. Parallel to the interface there exists a very thin δ-layer of dopants in the alloy region. Leaving immobile ionized dopants behind, electrons are then transferred from this δ-layer to the semiconductor interface where they form a uniform high-mobility two-dimensional electron gas (2DEG). The metallic gate is on the top surface of the wafer. By varying the applied gate voltage the electron density at the interface can be varied and even depleted. If the metallic gate is lithographically

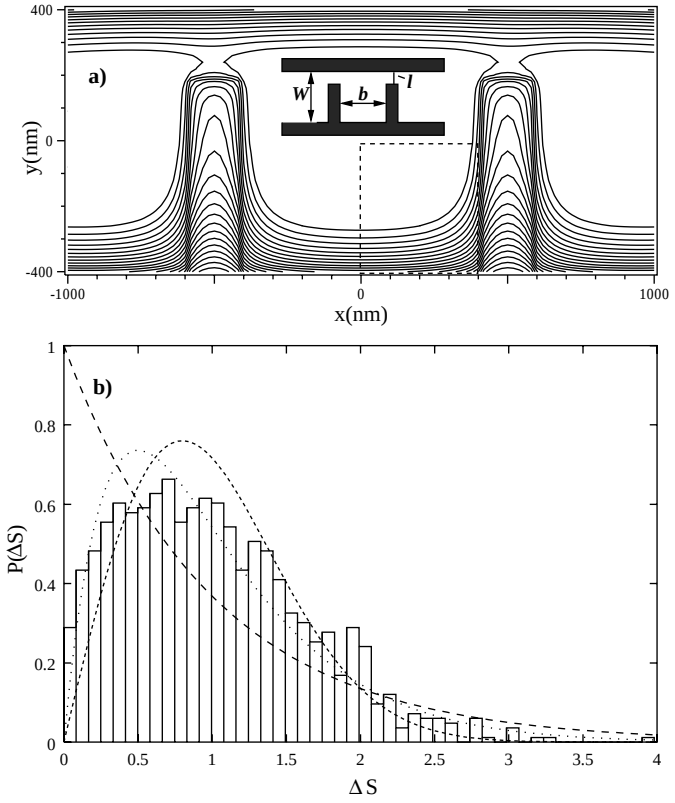

Fig. 1. (a) Contour plot of the potential resulting from self-consistent Thomas-Fermi calculations. The potential difference between each line is 8 meV. The density of positive charges $n_\mathrm{s} = 2 \times 10^{15}$ m^{-2}, the distance between the δ -layer and the 2DEG is 5 nm, the chemical potential $\mu = 5$ meV above the minimum of the potential, the dielectric constant $\epsilon = 13$, and the effective mass $m^* = 0.067 m_\mathrm{e}$ which are values for GaAs. The enclosed area is used to calculate level statistics. Inset is the model of the shape of the metal sheet that creates the quantum dot. In our calculations is $W = b = 800$ nm and $l = 200$ nm. (b) Level statistics of the enclosed area of the dot. The bars represent the probability to find states with normalized separation ΔS. The width of each bar is 5 μeV, the number of levels calculated is 1000, the highest energy 60 meV, and the dot is discretized in units of 2.5 nm. The long-dashed line is the Poisson distribution, the short-dashed line is the Wigner distribution and the dotted line is the Semi-Poisson distribution.

patterned, the electron gas can also be laterally confined and dots of various shapes may be created. In the present case we consider the lithographic pattern shown in the inset of Figure 1a, *i.e.*, a nominally square dot with narrow leads connecting to left and right reservoirs.

To obtain the effective potential of the 2DEG we have used a simple two layers model [25,26,22,27]. The two layers consist of the (smeared) positively charged δ-layer and the 2DEG itself. The pattern of the gate is projected directly onto the δ-layer. In the two layer model the positive charge under the gated regions is assumed to be canceled out by the gates. Effectively we therefore create a distribution of constant positive charge in the δ-layer having the same geometric shape as the ungated regions in the top metallic gate. Electric charge in the 2DEG is assumed to mirror the effective positive charge in the δ-layer. To first order the confining potential equals the bare potential V_c, that results from the positive charge only. Obviously this potential will be modified by the electrons occupying the device. Let this repulsive electrostatic potential be V_e. To find the total modified, self-consistent potential $V_\mathrm{c} + V_\mathrm{e}$ we have made use of the Thomas-Fermi approximation (TF) [28]. For many applications this method works well when used with the kinds of devices currently being studied as a result of their smooth features. The basic idea is that the system behaves locally as a homogeneous 2DEG with local density $\rho(\mathbf{r}_\parallel)$ and Fermi wave number $k_F(\mathbf{r}_\parallel)$ at position $\mathbf{r}_\parallel = (x, y)$. If μ is the overall chemical potential the following equality must be satisfied:

$$\frac{\hbar^2 k_\mathrm{F}^2(\mathbf{r}_\parallel)}{2m} + V_\mathrm{c}(\mathbf{r}_\parallel) + V_\mathrm{e}(\mathbf{r}_\parallel) = \mu. \tag{3}$$

The relation between the Fermi wave number and the local 2D density is

$$\rho(\mathbf{r}_\parallel) = \frac{k_\mathrm{F}^2(\mathbf{r}_\parallel)}{2\pi} \tag{4}$$

and the Hartree interaction term is

$$V_\mathrm{e}(\mathbf{r}_\parallel) = \frac{e^2}{4\pi\epsilon_0\epsilon} \int \frac{\mathrm{d}\mathbf{r}'_\parallel \rho(\mathbf{r}'_\parallel)}{|\mathbf{r} - \mathbf{r}'|}\,. \tag{5}$$

Initially for the iterative solution we set $V_\mathrm{e} = 0$ in equation (3), *i.e.*, effectively there are no electrons in the 2DEG. To avoid a numerical instability in consecutive iterations we use a combination of 5% of the new values and 95% of the previous ones to generate the next set of values for V_e to be inserted in equation (3). This is repeated until the potential has converged. The resulting potential is shown in Figure 1. The potential shown is connected to semi-infinite leads with the same transversal shape as the slice connecting to the leads. Obviously the effective confinement is much softer than the original lithographic one and is qualitatively similar to the potentials discussed by Stopa [27,15]. The potential is formed as a saddle-point at the constrictions, where it can be very well approximated with a harmonic potential in the y-direction, and a negative harmonic potential in the x-direction. In our calculations we obtain $\hbar\omega_x = 1.2$ meV and $\hbar\omega_y = 3.5$ meV, which are quite reasonable values [22,29–31].

3 Level statistics and the nature of the dynamics

As noted in the introduction, the dynamics of a nominally isolated square billiard, as in the inset in Figure 1a, is regular. One may then wonder if our refined self-consistent potential still supports the same type of dynamics or if the smoothing results in qualitatively new features, or more specifically, does the system turn into an irregular one. To investigate this issue we have considered the energy level

statistics [32] for the nominally isolated dot for $B = 0$. We thus apply the usual diagnostic tools in saying that if the nearest level separations ΔE follow the Poisson distribution

$$P(s) = \mathrm{e}^{-s}, \tag{6}$$

with $s = \Delta E/\langle \Delta E \rangle$, then the system is regular and has high probability of small level separations. On the other hand, if one finds the Wigner distribution

$$P(s) = \frac{\pi}{2} s \mathrm{e}^{-\frac{\pi}{4}s^2}, \tag{7}$$

then the dynamics is regarded as fully chaotic and levels repel each other. There are also a number of distributions for intermediate statistic, *e.g.*, Brody [33] and Berry-Robnik [34]. More recently the Semi-Poisson distribution

$$P(s) = 4s\mathrm{e}^{-2s} \tag{8}$$

is suggested by Gerland *et al.* [35] to have universal character, *i.e.*, when gradually changing from a chaotic to a regular system, the level statistics distribution always passes through the Semi-Poisson distribution at some point. The Semi-Poisson distribution shows level repulsion as the Wigner distribution but is more similar to the Poisson distribution for larger separations.

Because of the limited range of energy levels of interest here, we may use the rectangular area indicated in Figure 1a when characterizing the level spectrum. Among the four possible symmetries for the nominally isolated dot we have chosen the odd-odd symmetry [22], *i.e.*, wavefunctions must vanish at the boundaries indicated by dotted lines in the figure and have odd symmetry with respect to the x- and y-axes. The level spectrum was obtained by numerical discretization of the Schrödinger equation with $\Delta x = \Delta y = 2.5$ nm. About one thousand levels with energies less than ~ 60 meV relative the bottom of the cavity have been included in the histogram in Figure 1b. Evidently there is substantial level repulsion because the self-consistent potential is non-separable. As the figure also shows, the corresponding level statistics are rather close to the Wigner distribution. However, the latter do not fit exactly the calculated statistics, which indicates a mixed dynamics. Poincaré plots for the corresponding classical case confirm this picture. Thus we have obtained a system with chaotic features in spite of a regular lithography.

4 Conductance fluctuations

In this section we compute the conductance through the quantum dot modeled with the soft potential calculated in the previous section and compare it with the corresponding result for the hard-wall confinement. The zero-temperature conductance, $G(\epsilon, T = 0)$, is related to the total transmission coefficient, $T = \sum_{\alpha,\beta} |t_{\beta,\alpha}|^2$, by the Landauer formula $G(\epsilon, T = 0) = (2e^2/h)\, T$, where $|t_{\beta,\alpha}|^2$ is the transmission coefficient from the mode α in the entrance lead to the mode β in the exit lead at energy ϵ [1]. The effects of a finite temperature are accounted for in a standard way by the convolution of $G(\epsilon, 0)$ with the derivative of the Fermi-Dirac distribution, $f(E_\mathrm{F}, T)$, at the given Fermi energy, E_F, $G(E_\mathrm{F}, T) = -\int \mathrm{d}\epsilon G(\epsilon, 0) \partial f(\epsilon - E_\mathrm{F}, T)/\partial \epsilon$ [1]. The transmission coefficient T is calculated by solving a full quantum mechanical scattering problem for the potential shown in Figure 1. The semi-infinite wide channels to the right and left of the dot serve as source and drain. Hence the asymptotic scattering states are plane wave states propagating along the wide channels times the transverse states. The latter are obtained for the self-consistent potential of Figure 1 taken in the region far from the central dot ($x = \pm 1000$ nm). For the transport calculations here we make use of a hybrid recursive Green-function technique in which the magnetic field is included both in the leads and the dot regions [36]. The accuracy of the numerical method has been checked with a single quantum point contact where the results for the total transmission are found to be in excellent agreement with analytic results [37].

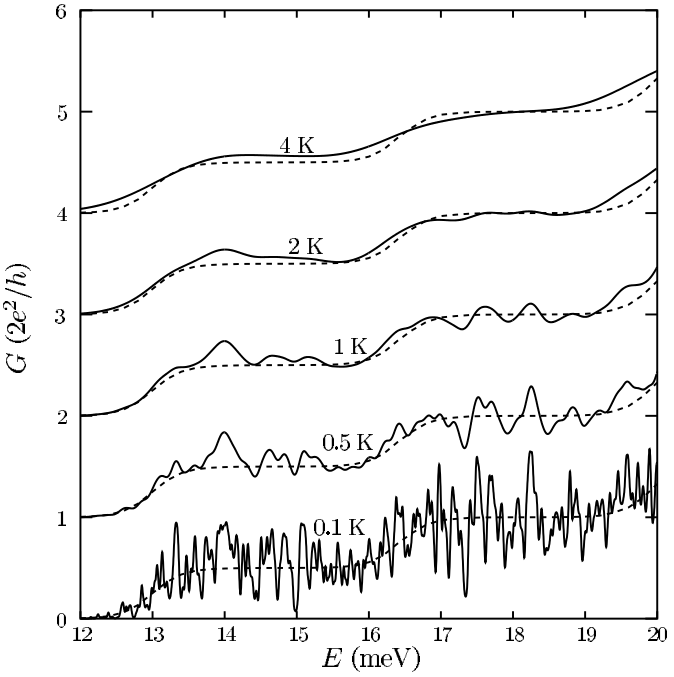

Fig. 2. Calculated conductance *vs.* energy for different temperatures and at zero magnetic field. The solid lines are the temperature averaged curves for the quantum dot and the dashed lines are half the conductance for single quantum point contact. The curves have been offset for clarity

Figure 2 shows the calculated conductance of the quantum dot as a function of the Fermi energy at different temperatures and at zero magnetic field. The zero-temperature conductance exhibits characteristic ballistic fluctuations caused by interference of phase-coherent electrons inside the dot. As the temperature increases, the ballistic fluctuations are gradually smeared out. At $T \equiv T_\mathrm{Ohmic} \gtrsim 2$ K the conductance of the dot approaches

its Ohmic value corresponding to the addition of the resistances of the two individual quantum point contacts (QPC) defining the dot, $G^{-1}_{\rm Ohmic} = 2G^{-1}_{\rm QPC}$. Obviously, the Ohmic addition of the resistances is already achieved by the temperature (energy) averaging of the phase-coherent electrons, *i.e.*, inelastic processes are yet to be included.

Conductance oscillations in a dot of the same size but in a hard-wall confinement model was studied in reference [24]. It was found that the conductance approaches its Ohmic value at the same temperatures $T \gtrsim 2$ K. Experimentally, however, the Ohmic addition is shown to occur at somewhat lower temperatures [38]. It was argued [24] that this difference in the temperature may be attributed to the effect of the soft confinement which might be an additional factor to the temperature smearing which makes the conductance oscillations weaker. For example, the conductance of a single QPC with hard wall confinement exhibits rapid fluctuations (superimposed on the conductance steps) due to the mixing of modes inside and outside the QPC [1,39]. When a realistic model of a soft parabolic confinement is used, the mode mixing is strongly suppressed and these conductance fluctuations disappear [37]. However, in contrast to a single QPC, the results of the present numerical calculations for the quantum dots demonstrate that soft confinement has apparently little effect on the smearing of fluctuations in comparison to the hard-wall case. This can be understood as follows. As shown by explicit transport calculations of the type used here, transport through the open dot is effectively mediated by eigenstates of the corresponding closed structure [40–42]. This is also an underlying basic assumption in the RM theory [43]. This implies that incoming and reflected states are coupled to several eigenstates of the dot so that a strong mode mixing inevitably occurs. The resulting transmission coefficient will be governed by the interference of the states inside the dot and by the strength of coupling of the wave function near the openings to the states in the leads. In contrast, in a single QPC the transmission is determined by the number of propagating modes in its narrowest part. In the case of a realistic parabolic confinement, the potential is separable. As a result, transport is adiabatic (no mode mixing occurs in the narrowest part of the QPC) and therefore the conductance fluctuations are suppressed.

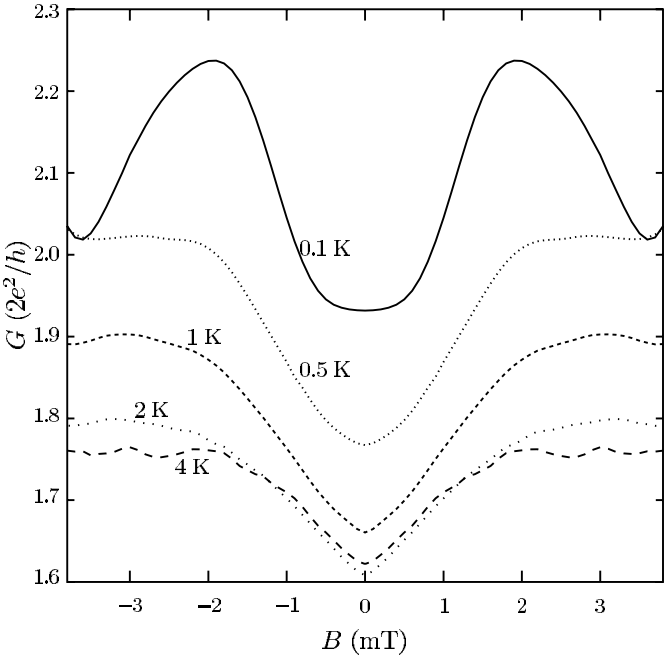

Fig. 3. Calculated conductance *vs.* magnetic field, varying temperature and keeping the energy constant at 21.5 meV (three open channels).

5 Temperature-averaged weak localization

5.1 Numerical calculations

In this section we perform a numerical study of the temperature-averaged WL of a quantum dot with a realistic soft confinement. It was shown previously that the semiclassical prediction for the energy-averaged WL peak becomes applicable for a *single* device in the limit of elevated temperature when Ohmic behavior is established in the dot [24]. In turn, the Ohmic behavior (*i.e.* $G^{-1}_{\rm Ohmic} = 2G^{-1}_{\rm QPC}$, see previous section) implies that the electron velocity distribution in the dot is effectively randomized by multiple boundary reflections and averaging over a wide energy interval, due to the effect of the finite temperature. This means that the temperature averaging provides the energy averaging required by the semiclassical theory. We stress here that performing the temperature averaging we completely disregard inelastic processes (electron-electron interaction etc.). The latter cause the loss of the phase coherence at elevated temperatures. However, we demonstrate below that for real systems one can still study the temperature averaged WL in a single device at sufficiently low temperatures when the dephasing does not completely destroy coherent motion.

Figure 3 shows a representative magnetoresistance of the dot with the potential of Figure 1a for different temperatures. The Fermi energy is set to 21 meV which corresponds to 3 propagating modes in the constrictions. For low temperatures ($T \lesssim 0.5$ K) the magnetoresistance does not exhibit any regular features, being strongly sensitive to minute variations of the Fermi energy. As the temperature is increased above the limit set by the Ohmic behavior (*i.e.* $\sim$2 K for the dot under consideration), ballistic fluctuations are smeared out and the shape of the curve does not undergo any further significant changes. The WL correction, that results from the temperature smearing, is reduced from $\Delta R \sim 0.21$ at $T = 1$ K to $\Delta R \sim 0.12$ at $T = 4$ K. These trends in the temperature behavior of the magnetoresistance of the quantum dot with soft confinement is qualitatively similar to that of an idealized square quantum dot with a hard-wall potential [24].

The WL lineshapes at fixed temperature but for different number of modes, N, in the constrictions are shown in Figure 4. In our calculations we use a fixed potential, Figure 1a, and change N by changing the Fermi

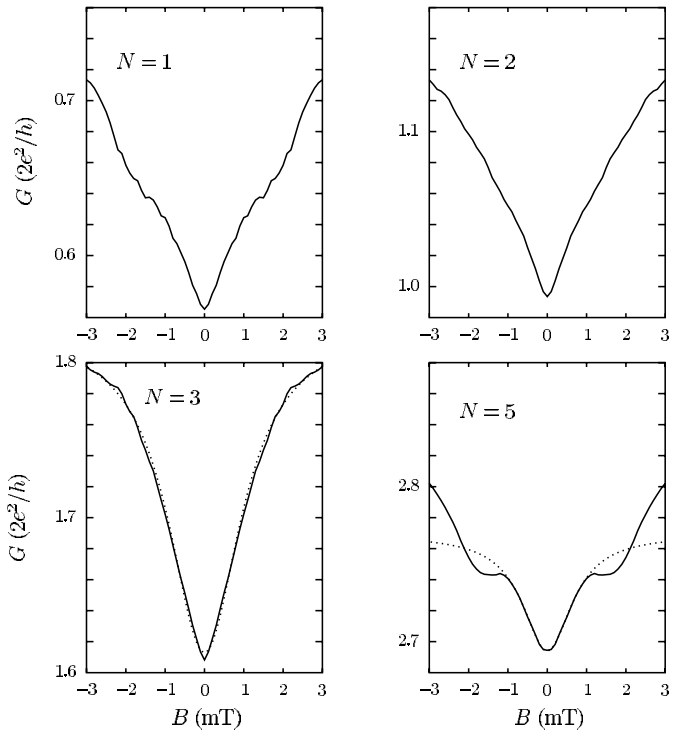

Fig. 4. Calculated conductance *vs.* magnetic field, varying the number of open channels and keeping the temperature constant at 2 K. The energies are 14.5 meV, 18.0 meV, 21.5 meV, and 28.5 meV for $N = 1$, 2, 3, and 5 respectively. The dashed lines for $N = 3$ and $N = 5$ are Lorentzian fits.

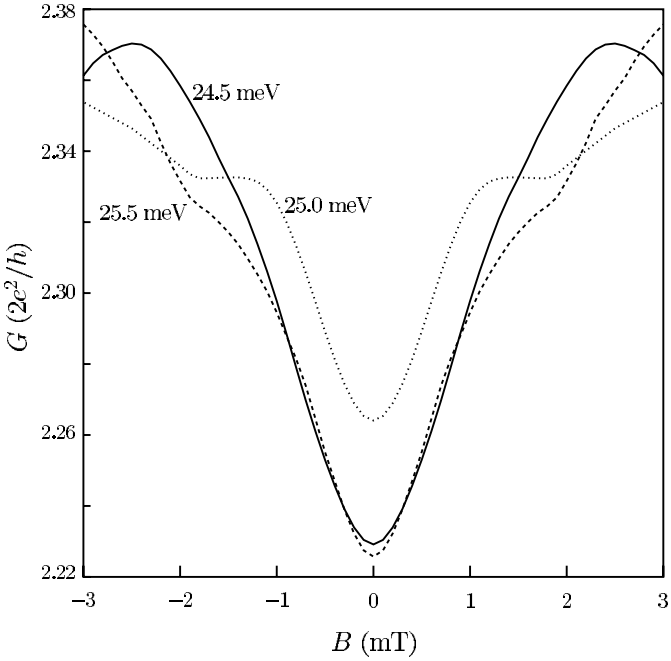

Fig. 5. Calculated conductance *vs.* magnetic field with $N = 4$ for three different energies at $T = 2$ K.

energy of incoming electrons. Note that the lineshape of the temperature-averaged WL peak remains rather similar as long as the Fermi energy lies in a range where the number of propagating modes in the leads does not change (Fig. 5). When the number of open channels in the leads is set to one and two, $N = 1, 2$, the conductance increases rather (quasi-)linearly and no Lorentzian fit to the WL lineshape is possible. If the number of conducting channels is greater or equal to three, the WL lineshape is well-described by a Lorentzian. (However, in many cases the Lorentzian lineshape is distorted by a characteristic "shoulder" structure which is also seen in the experiment, Fig. 4). When $N = 4, 5$ the best fit to equation (1) gives a typical area S which is in rather good agreement ($\sim 15\%$) with the effective area of the dot. This is similar to a square dot with hard walls where the linear lineshape is evident for $N \geq 3$ [24]. Note, that according to the RMT-approach [8] no WL correction ($\Delta R = 0$) is expected for the structures under consideration, which have a reflection symmetry through an axis perpendicular to the current. Numerical calculations show that this does not hold for the dot at hand, $\Delta R = 0.15 \sim 0.2$ when $N = 1 \sim 3$. However, ΔR decreases with increased number of modes, $\Delta R = 0.05 \sim 0.06$ for $N = 4, 5$.

We conclude this section with a brief discussion of the effect of direct trajectories connecting the entrance and exit leads. Such trajectories may be responsible for non-universal features in the conductance [2]. In experiments these trajectories are often eliminated by adding a stopper which blocks the directly transmitted path. However, for the structure under consideration the effect of these trajectories is negligible. This is because the incoming electrons enter the dot in a collimated beam directed over the diagonal of the dot due to a classical horn collimation effect [41]. As a result, only a small fraction of the incoming electron exit the dot without first being scattered off the walls.

5.2 Experiment

The inset of Figure 6 contains a micro-graph of an identical device to the one used in these measurements. The dot was defined electro-statically by means of four gates which were deposited on a high mobility AlGaAs/GaAs wafer. The bulk 2DEG mobility (density) ranged between 2×10^6 cm^2/Vs (1.7×10^{11} cm^{-2}) and 4.3×10^6 cm^2/Vs (3.3×10^{11} cm^{-2}) depending on the amount of illumination with a red light emitting diode. The 2DEG was positioned 95 nm below the top surface of the wafer. The four gates performed the following roles. One gate defined the right hand edge of the dot. Two finger gates defined the entrance and exits of the dot while the fourth gate (the plunger gate) defined the left hand edge of the dot. The finger gates were used to control the number of modes in the entrance and exit leads whilst the plunger gate was used to control the width of the dot. A nominal size of the dot was 450×490 nm. Edge state backscattering techniques were used to determine the number of modes in the entrance and exit leads as a function of the voltage applied to either the finger or plunger gate voltage for

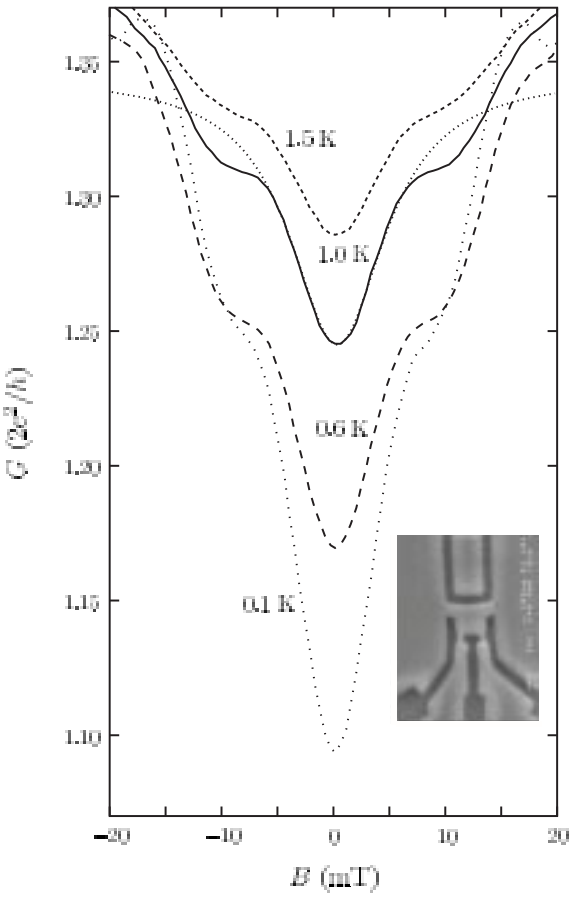

Fig. 6. Experimental conductance *vs.* magnetic field for three open channels and different temperatures. The dotted line is a Lorentzian fit to the $T = 1.0$ K curve. Inset is the experimental device.

a fixed voltage applied to the right hand gate. These measurements were repeated for different temperatures for a configuration in which there were three modes in the constrictions.

Measurements were made on a dilution refrigerator using standard low frequency AC techniques. The temperature was varied between 0.1 K and 1.5 K. These temperatures are lower than the calculated $T_{\mathrm{Ohmic}} \approx 2$ K. We choose the lower temperature to reduce the effects of inelastic scattering which may be important in a real dot at elevated temperatures $T \gtrsim 1$K. Figure 6 shows the conductance versus magnetic field for different temperatures with the number of open channels $N = 3$. For all temperatures the WL peak has a Lorentzian lineshape giving an effective area (according to Eq. (1)) $S \approx 6.5 \times 10^{-14}$ m^2. The lithographical area is $S_{\mathrm{lith}} \approx 1.6 \times 10^{-13}$ m^2, which gives a typical area which is about 40% of the actual one. This is consistent with our numerical model for the case of three modes in the leads where the same relation is about 35%. The magnitude of the WL correction is decreasing with increasing temperature from $\Delta R \sim 0.15$ at $T = 100$ mK to $\Delta R \sim 0.04$ at $T = 1.5$ K. All values are between the RMT predictions $\Delta R = 0$, expected for structures with reflection symmetry through an axis perpendicular to the current, and $\Delta R = N/(4N + 2) = 0.21$ when $N = 3$, for asymmetric structures. Note that the temperature dependence of the amplitude of the experimental WL corrections is in good agreement with the calculated one.

5.3 Discussion

One of the most striking findings of the numerical calculations on the temperature averaged WL is that the same (chaotic) quantum dot generates both linear and Lorentzian lineshape of the WL depending on the lead conditions (*i.e.* number of available open channels).

In order to understand this feature and its relations to the semiclassical [2] and the RMT predictions we recall the main assumptions used in the above theories. The key points in the semiclassical approach [2] is the exponential distribution of the classical areas A enclosed by a classical path in chaotic structures,

$$P(A) \sim \mathrm{e}^{-\alpha|A|}, \tag{9}$$

and the assumption of uniformity (the area distribution does not depend on the incident angle). For the regular structure, the area distribution is characterized by the power law

$$P(A) \sim A^{-\beta} \tag{10}$$

for large A and it depends on the incident angle of the particle. The difference between these two distributions yields different lineshapes of the WL peak as given by equations (1, 2). Classical numerical simulations confirm the above conjectures on the area distribution for a number of chaotic and regular structures [2,44,45]. However, classical simulations also demonstrate that the above distributions are sensitive to the lead positions and details of the structure. In particular, for the same stadium billiard, both the exponential and the power-law distribution were obtained. Which one depends on the particular position of the leads [45]. The algebraic distribution (10) was also found in the stadium-shaped quantum dot with a soft confinement [23], the chaotic system with a mixed phase space. In addition, a pronounced deviation from equation (9) at small areas has been found for the antidot arrays embedded in a square [16], the system which classically exhibits hard chaos. This deviation (related to the specific short-time trajectories in the structure) was shown to lead to the non-universal features in the WL lineshape.

The exponential distribution of the classical areas in the chaotic cavity is a consequence of the classical exponential escape probability via a hole [46],

$$P(t) \sim \mathrm{e}^{-\gamma t}, \tag{11}$$

where the escape rate γ is related to the parameter α, $\alpha \propto \sqrt{\gamma}$ (see [44] for detailed calculations of γ and α for different structures). In contrast, the escape probability in a classical regular cavity is given by the slower power-law dependence,

$$P(t) \sim t^{-\xi}. \tag{12}$$

Numerous classical numerical simulations [46,2,44,45] have confirmed the exponential and the power-law decays in correspondingly chaotic and regular systems, although a significant deviation [47] from (11) and even a crossover to the delayed power-law escape rate for the chaotic billiards was detected [48,23]. The possibility of the power-law area distribution and the delayed algebraic decay in the classical chaotic system is related to the existence of the marginally stable periodic orbits where a particle can be trapped for a long time.

However, recent theoretical and experimental studies [48,49] show that the decay in a corresponding *quantum* system is qualitatively different from its classical counterpart. Namely, the probability that the quantum system decays at time t after its formation is

$$P(t) \sim t^{-2-M/2}, \tag{13}$$

where M is the number of the open channels. Note that the difference between (13) and (11) is not due to the existence of the marginally stable periodic orbits (which may cause an algebraically delayed escape rate even in a classically chaotic system as was discussed above), but a consequence of the quantum dynamics. Thus, because of the qualitative difference in the escape probability in the classical and corresponding quantum mechanical systems it is not quite clear to what extent one can justify equation (9) (which essentially relies on the classical exponential decay law (11)) in the description of the coherent electron dynamics in the *quantum* system.

It is important to stress that the WL corrections (1, 2) are derived within a framework of a diagonal approximation using a stationary phase approximation for the evaluation of semiclassical Green functions. The diagonal approximation implies that only trajectories with the same entrance and exit angle, of electrons propagating in the same mode in the leads, contribute to the WL corrections. It has been noted [2], however, that in some cases the off-diagonal contribution may be comparable [10] or even dominate the diagonal ones, leading to positive corrections to the classical magnetoresistance. Besides, the stationary phase approximation is shown to be invalid in the case of a low mode number [10,47], *i.e.*, in the case relevant to most experiments.

It is difficult to say which of the above mentioned factors plays a dominant role in the discrepancy between the semiclassical predictions (1, 2) and the exact numerical calculations for the device at hand. Nevertheless, any of the above factors (not included in the initial assumption used in derivation of (1, 2)) may significantly modify the WL corrections of a specific structure used in the experiment. Thus, in our opinion, the detection of the Lorentzian or linear lineshape in a particular cavity does not necessary mean that the corresponding dynamics is chaotic or regular. Instead, the observed dependencies may rather reflect specific features of the geometry under consideration such as existence of non-universal short-time orbits, effects of mixed dynamics, the lead position, etc. This conclusion is supported by a number of experimental observations. Indeed, as discussed in the introduction, in most of the experiments performed to date there is no apparent correlation between the observed lineshape of the WL and the expected one. In particular, for the case of $N = 3$ modes in the leads our numerical calculations (showing the Lorentzian lineshape) are in agreement with our experimental data as well as with the results reported by Lütjering *et al.* [16]. The linear lineshape seen in the calculations for a low number of modes are in accordance to the data reported by Bird *et al.* [14] for $N = 2$ for a similar dot. However, in contrast to our numerical results, the square dots generated the linear lineshape for $N = 2, 3$ in experiments of Lee *et al.* [18] as well as the Lorentzian one for $N = 2$ as reported by Chan *et al.* [13]. Different WL lineshapes observed in nominally identical circular devices [11,12,18] further stress the fragile character of these dependencies and their extreme sensitivity to the non-universal features related to the existence of characteristic periodic orbits, different lead coupling, chosen energy interval, impurity configurations etc. When many modes are occupied, the numerical results are in better agreement with the semiclassical predictions, which is also consistent with the basic assumptions made in the original derivation of the lineshape. However, it should be noted that most of the experiments reported to date refer to the case of a few mode regime in the leads.

Now let us focus on the RMT approach to the WL corrections [3–9]. In this approach the scattering $S-$matrix is constructed on the basis of the appropriate statistical ensemble. The RMT predicts the Lorentzian shape of the WL corrections for any number of modes in the leads including $N = 1$ and any strength of the coupling between the leads and the dot [6,9]. It is important to stress, however, that the RMT is valid for a completely chaotic dot and it does not take into account any system-specific features and completely disregards the effects of non-universal characteristic related to the short periodic orbits etc. (Note that the recent work of Prange [50] attempts to incorporate the knowledge of short periodic orbits into the RMT approach). Therefore, direct application of the RMT to many systems where periodic orbits are known to play an important role (like, for example, square, circular, stadium quantum dots) can not be justified. This is probably the case for the dot under consideration (with regular component of motion being present) where neither experimental nor numerical calculated WL corrections agree with the RMT predictions. As both the temperature and the WL correction are averaging effects there should be no need to take temperature into account in the RMT predictions [7]. However, the numerical and experimental results described above, show a significant dependence on temperature for the WL correction. For low temperatures the averaging is not large enough to make the averaging in the RMT valid. When the temperature is close to $T_{\rm Ohmic}$ the WL correction is reduced, but still significant.

Recently the RMT was used to describe an inelastic scattering in the dot [7] on the basis of the Büttiker model [51] of a fictitious lead with N_ϕ phase-breaking channels. Within this approach N_ϕ is a phenomenological

parameter of the theory which can be determined by the comparison of the experimentally observed WL correction to the theoretical one, $\Delta G \approx -N/2(2N + N_\phi)\,(2e^2/h)$. This means that any deviations from the RMT predictions where inelastic scattering is not included are attributed to the effect of the phase-breaking processes. However, as shown above, the magnitude of the WL correction can be strongly sensitive to the shape-specific features of the dot. Thus, the above deviations can simply reflect the geometry-specific characteristics and be unrelated to the inelastic scattering inside the dot, such that the value of N_ϕ extracted from the ΔG can be rather misleading.

6 Conclusions

The conductance including the weak localization correction of a nominally square quantum dot has been studied both theoretically and experimentally. The confinement induced by remote gates has been modeled on the basis of the self-consistent Thomas-Fermi approximation. The resulting confining potential is shown to give rise to considerable level repulsion which is an indication of the chaotic dynamics inside the dot. This is in contrast to the regular dynamics in a square billiard with hard-wall boundaries.

The resulting soft potential is then used in full quantum-mechanical transport calculations. It was shown that, in contrast to previous conjectures, the soft confinement has no apparent effect on the smearing of the conductance fluctuations in comparison to the hard-wall scenario. The physical explanation for this is given.

Numerical calculations have been carried out to investigate a temperature averaged weak localization in the dot. One of the most striking findings of the numerical calculations on the temperature averaged WL is that the same (chaotic) quantum dot generates both linear and Lorentzian lineshape of the WL depending on the lead conditions (*i.e.* number of available open channels). We also present experimental WL data for a lithographically square dot and compare the results with numerical calculations. We find that the semiclassical and the random matrix theory predictions of the shape and the magnitude of the weak localization corrections are not always in agreement with our findings. The discrepancy is especially pronounced for the case of a few open channels. A critical analysis of the above theories is given with a particular emphasis of their application to real dots studied in today's experiments. Our results suggest that the lineshape of the WL (Lorentzian or linear) does not necessary reflect the character of underlying electron dynamics (chaotic or regular) but may rather be related to geometry-specific features of the dot. We therefore conclude that direct application of the semiclassical and RMT predictions, equations (1, 2), to distinguish between chaotic and regular dynamics in a particular cavity can not always lead to reliable conclusions as the shape and magnitude of the WL correction can be strongly sensitive to the shape-specific features of the dot.

We would like to thank P. Münger for help with parallel programming on the Cray T3E supercomputer, the National Supercomputer Centre in Linköping University for computational resources, Y. Feng and Z. Wasilewski for experimental devices, and the Swedish Natural Research Council and Swedish Research Council for Engineering Sciences for partial financial support.

References

1. C.W.J. Beenakker, H. van Houten, in *Solid State Physics, Advances in Research and Applications*, edited by H. Ehrenreich, D. Turnbull (Academic, San Diego, 1991), Vol. 44.
2. H.U. Baranger, R.A. Jalabert, A.D. Stone, Phys. Rev. Lett. **70**, 3876 (1993); H.U. Baranger, R.A. Jalabert, A.D. Stone, Chaos **3**, 665 (1993).
3. for a review of the random matrix theory see, *e.g.*, C.W.J. Beenakker, Rev. Mod. Phys. **69**, 731 (1997).
4. H.U. Baranger, P.A. Mello, Phys. Rev. Lett. **73**, 142 (1994);
5. R.A. Jalabert, J.-L. Pichard, C.W.J. Beenakker, Europhys. Lett. **27**, 255 (1994).
6. Z. Pluhař, H.A. Weidenmüller, J.A. Zuk, C.H. Lewenkoff, Phys. Rev. Lett. **73**, 2115 (1994); Z. Pluhař, H.A. Weidenmüller, J.A. Zuk, C.H. Lewenkoff, F.J. Wegner, Ann. Phys. (N.Y.) **243**, 1 (1995).
7. H.U. Baranger, P.A. Mello, Phys. Rev. B. **51**, 4703 (1995).
8. H.U. Baranger, P.A. Mello, Phys. Rev. B. **54,** R14297 (1996).
9. U. Gerland, H.A. Weidenmüller, Europhys. Lett. **35**, 701 (1996).
10. W.A. Lin, R.V. Jensen, Phys. Rev. B **53**, 3638 (1996).
11. A.M. Chang, H.U. Baranger, L.N. Pfeiffer, K.W. West, Phys. Rev. Lett. **73**, 2111 (1994).
12. M.J. Berry, J.A. Katine, R.M. Westervelt, A.C. Gossard, Phys. Rev. B **50**, 17721 (1994).
13. I.H. Chan, R.M. Clarke, C.M. Marcus, K. Campman, A.C. Gossard, Phys. Rev. Lett. **74**, 3876 (1995).
14. J.P. Bird, K. Ishibashi, D.K. Ferry, Y. Ochiai, Y. Aoyagi, T. Sugano, Phys. Rev. B **52**, 8295 (1995).
15. J.P. Bird, D.M. Olatona, R. Newbury, R.P. Taylor, K. Ishibashi, M. Stopa, Y. Aoyagi, T. Sugano, Y. Ochiai, Phys. Rev. B **52**, 14336 (1995).
16. G. Lütjering, K. Ritcher, D. Weiss, J. Mao, R.H. Blick, K. von Klitzing, C.T. Foxon, Surf. Sci. **361/362**, 709 (1996).
17. M.W. Keller, A. Mittal, J.W. Sleight, R.G. Wheeler, D.E. Prober, R.N. Sacks, H. Shtrikmann, Phys. Rev. B **53**, R1693 (1996).
18. Y. Lee, G. Faini, D. Mailly, Phys. Rev. B **56**, 9805 (1997).
19. M. Brack, R.K. Bhaduri, *Semiclassical Physics* (Addison-Wesley, Reading, Mass., 1997).
20. D.K. Ferry, S.M. Goodnick, *Transport in Nanostructures* (Cambridge University Press, Cambridge, 1997).
21. In reference [18] a nominally (lithographically) square quantum dot with a stopper preventing direct paths between leads was considered as non-chaotic. Numerical analysis of the nearest neighbor level spacing statistic for the actual self-consistent potential shows that the statistics are close to the Wigner distribution, *i.e.* dot is chaotic, see below for details.

22. K.-F. Berggren, Z.-L. Ji, Chaos **6**, 543 (1996).
23. R. Ketzmerick, Phys. Rev. B **54**, 10841 (1996); A.S. Sachrajda, R. Ketzmerick, C. Gould, Y. Feng, P.J. Kelly, A. Delage, Z. Wasilewski, Phys. Rev. Lett. **80**, 1948 (1998).
24. I.V. Zozoulenko, K.-F. Berggren, Phys. Rev. B **54**, 5823 (1996).
25. J.A. Nixon, J.H. Davies, Phys. Rev. B **41**, 7929 (1990).
26. M.J. Laughton, J.R. Barker, J.A. Nixon, J.H. Davies, Phys. Rev. B **44**, 1150 (1991).
27. M. Stopa, Phys. Rev. B **54**, 13 767 (1996).
28. R.G. Parr, W. Yang, *Density-Functional Theory of Atoms and Molecules* (Oxford University Press, New York, 1989).
29. L. Martin-Moreno, J.T. Nicholls, N.K. Patel, M. Pepper, J. Phys.-Cond. Matter **4**, 1323 (1992).
30. N.K. Patel, J.T Nicholls, L. Martin-Moreno, M. Pepper, J.E.F. Frost, D.A. Ritchie, G.A.C. Jones, Phys. Rev. B **44**, 13 549 (1991).
31. R. Taboryski, A. Kristensen, C.B. Sørensen, P.E. Lindelof, Phys. Rev. B **51**, 2282 (1995).
32. M. Gutzwiller, *Chaos in Classical and Quantum Mechanics* (Springer-Verlag, New York, 1991).
33. T.A. Brody, Lett. Nuovo Cimento **7**, 482 (1973).
34. M.V. Berry, M. Robnik, J. Phys. A **30**, 8787 (1984).
35. U. Gerland, *Quantum Chaos and Disordered Systems: How close is the analogy?*, Dissertation, Ruprecht-Karls-Universität, Heidelberg (1998); E. Bogomolny, U. Gerland, C. Schmit, Phys. Rev. E **59**, 2956 (1999).
36. I.V. Zozoulenko, F.A. Maaø, E.H. Hauge, Phys. Rev. B **53**, 7975 (1996); **53**, 7987 (1996); F.A. Maaø, I.V. Zozoulenko, E.H. Hauge, *ibid.* **50**, 17 320 (1994).
37. M. Büttiker, Phys. Rev. B **41**, 7906 (1990).
38. L.P. Kouwenhoven, B.J. van Wees, W. Kool, C.J.P.M. Harmans, A.A.M. Staring, C.T. Foxon, Phys. Rev. B **40**, 8083 (1989).
39. G. Kirczenow, Phys. Rev. B **39**, 10 452 (1989).
40. K.-F. Berggren, Z.-L. Ji, T. Lundberg, Phys. Rev. B **54**, 11612 (1996).
41. I.V. Zozoulenko, R. Schuster, K.-F. Berggren, K. Ensslin, Phys. Rev. B **55**, R10 209 (1997).
42. I.V. Zozoulenko, K.-F. Berggren, Phys. Rev. B **56**, 6931 (1997).
43. See, *e.g.*, Y. Alhassid, H. Attias, Phys. Rev. B **54**, 2696 (1996) and references cited.
44. R.V. Jensen, Chaos **1**, 101 (1991).
45. W.A. Lin, J.B. Delos, R.V. Jensen, Chaos **3**, 655 (1993).
46. W. Bauer, G.F. Bertsch, Phys. Rev. Lett. **65**, 2213 (1990).
47. H. Ishio, J. Burgdörfer, Phys. Rev. B **51**, 2013 (1995).
48. H. Alt, H.-D. Gräf, H.L. Harney, R. Hofferbert, H. Lengeler, A. Ritcher, P. Schardt, H.A. Weidenmüller, Phys. Rev. Lett. **74**, 62 (1995); H. Alt, H.-D. Gräf, H.L. Harney, R. Hofferbert, H. Rehfeld, A. Ritcher, P. Schardt, Phys. Rev. E **53**, 2217 (1996).
49. P. Seba, K. Życzkowski, J. Zakrzewski, Phys. Rev. E **54**, 2438 (1996).
50. R.E. Prange, Phys. Rev. Lett. **77**, 2447 (1996).
51. M. Büttiker, Phys. Rev. B **33**, 3020 (1986).